

Absolute Rate Coefficient of the OH + CH₃C(O)OH Reaction at *T* = 287–802 K. The Two Faces of Pre-reactive H-Bonding

Victor G. Khamaganov,[†] Vung Xuan Bui, Shaun A. Carl, and Jozef Peeters*

Department of Chemistry, University of Leuven, Celestijnenlaan 200 F, 3001 Leuven, Belgium

Received: August 1, 2006; In Final Form: September 21, 2006

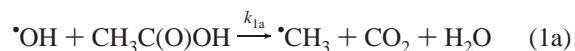
The rate constants for the reaction OH + CH₃C(O)OH → products (1) were determined over the temperature range 287–802 K at 50 and 100 Torr of Ar or N₂ bath gas using pulsed laser photolysis generation of OH by CH₃C(O)OH photolysis at 193 nm coupled with OH detection by pulsed laser-induced fluorescence. The rate coefficient displays a complex temperature dependence with a sharp minimum at 530 K, indicating the competition between a reaction proceeding through a pre-reactive H-bonded complex to form CH₃C(O)O + H₂O, expected to prevail at low temperatures, and a direct methyl-H abstraction channel leading to CH₂C(O)OH + H₂O, which should dominate at high temperatures. The temperature dependence of the rate constant can be described adequately by $k_1(287\text{--}802\text{ K}) = 2.9 \times 10^{-9} \exp\{-6030\text{ K}/T\} + 1.50 \times 10^{-13} \exp\{515\text{ K}/T\}$ cm³ molecule⁻¹ s⁻¹, with a value of $(8.5 \pm 0.9) \times 10^{-13}$ cm³ molecule⁻¹ s⁻¹ at 298 K. The steep increase in rate constant in the range 550–800 K, which is reported for the first time, implies that direct abstraction of a methyl-H becomes the dominant pathway at temperatures greater than 550 K. However, the data indicates that up to about 800 K direct methyl-H abstraction remains adversely affected by the long-range H-bonding attraction between the approaching OH radical and the carboxyl –C(O)OH functionality.

1. Introduction

In recent years, much attention has been focused on the atmospheric chemistry of organic acids primarily because of their contribution to the acidity of atmospheric precipitation. In particular, the monocarboxylic acids, acetic acid and formic acid, are responsible for most of the acidification in remote regions,¹ with the former generally being found with the highest concentrations. Acetic acid has wide and diverse sources: direct input to the atmosphere from biomass burning,² vehicle exhausts,³ vegetation and soil,^{4,5} and snow packs⁶ have been reported. Several atmospheric sources of acetic acid have also been proposed. Some of these were incorporated recently by Warneck⁷ in a box model study of C₂ and C₃ organic species, including acetic acid, in the marine atmosphere. In that study, the dominant production routes for acetic acid in the gas phase were given as the following: reaction of OH with acetone, reaction of HO₂ with the acetyl peroxy radical, and reaction of propene with ozone, and in the liquid phase, reaction of OH with acetone, decomposition of peroxyacetyl nitrate (CH₃CO(O)ONO₂), and reaction of ethane peroxy acid (CH₃CH(O)OOH) with hydrogen sulfite (HSO₃⁻). However, the first of these, gas-phase production via OH + acetone, should be a very minor source of acetic acid given the recent findings of a very small branching fraction to this product channel (a few percent)^{8,9} in contradiction to the study of Wollenhaupt et al.¹⁰ on which the rate constant value used by Warneck is based. However, a new acetic-acid-forming route initiated by the HO₂ + acetone reaction at tropopause temperatures has been proposed recently by Hermans et al.¹¹ The main removal route for acetic acid is likely to be dry¹² and wet⁷ deposition and,

during the day, also gas-phase reaction with OH, given that most atmospheric acetic acid is found in the gas phase.

The reaction of OH with acetic acid may proceed by two hydrogen abstraction channels:



Under atmospheric conditions, the CH₃C(O)O• intermediate initially formed in channel 1a is expected to decompose to CH₃ and CO₂ on a nanosecond time scale, the barrier being only ~5 kcal/mol.¹³ The recent studies of reaction 1 by Butkovskaya et al.¹⁴ and De Smedt et al.¹⁵ agree on a large branching fraction to channel 1a at room temperature: $k_{1a}/k_1 = 0.64 \pm 0.17$ and 0.64 ± 0.14 , respectively. At first sight, one might expect the preference of channel 1b given that the C–H bond dissociation energy in the methyl group of CH₃C(O)OH is ~12 kcal/mol¹⁵ less than that of O–H at the carboxyl site. The first indication of the preference of channel 1a at atmospheric temperatures came from the study by Singleton et al.¹⁶ who observed a significant decrease in reactivity upon D substitution at the carboxyl site but not upon D substitution at the methyl group. The observed negative temperature dependence for k_1 in that study was attributed to the formation of a pre-reactive complex. Moreover, the negative temperature dependence of k_1 also found by Butkovskaya et al.¹⁴ and the theoretical study by Vereecken et al.¹⁵ support and confirm, respectively, the idea of a pre-reactive six-ring complex with OH doubly H-bonded to the carboxyl group (see Figure 8), followed by abstraction of the acidic H-atom enhanced by tunneling. Contrary to these findings is the slightly positive temperature dependence of k_1 reported by Dagaut et al.¹⁷ for the range $T = 298\text{--}440$ K. The current

* Corresponding author. E-mail: jozef.peeters@chem.kuleuven.be.

[†] Currently at Max Planck Institut, Mainz, Division of Atmospheric Chemistry.

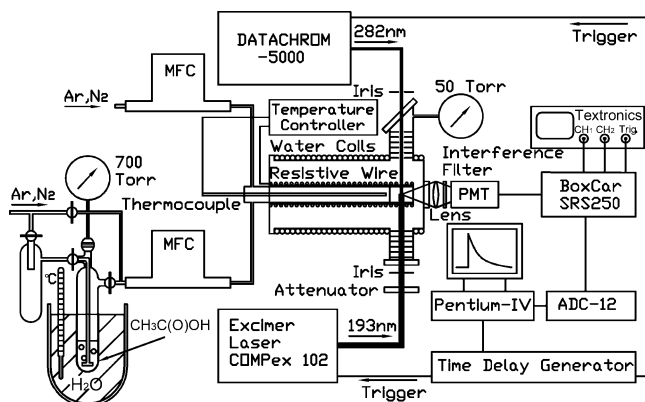


Figure 1. PLP–PLIF experimental setup. PMT, photomultiplier; boxcar, signal integrator and averager; MFC, mass flow controllers; IF, 309 nm interference filter; DATACHROM-5000, laser light source (200–1000 nm) from Quantel Corp. consisting of Nd:YAG–dye laser combination including wavelength extender; TEKTRONICS, 2-channel oscilloscope.

recommendation for the 298 K rate constant and the temperature dependence by the NASA data evaluation panel¹⁸ represents an average of the data of Singleton et al.¹⁶ and Dagaut et al.,¹⁷ resulting in a weak negative temperature dependence. However, the IUPAC¹⁹ recommendation is based on the results of Singleton et al.¹⁶ and Butkovskaya et al.¹⁴ and therefore results in a much more pronounced negative temperature dependence.

One complication in gas-kinetic measurements on acetic acid is the presence of relatively large fractions of the dimer at lower temperatures, as was observed in the study of Singleton et al.¹⁶ involving fairly high acetic acid concentrations. The eight-membered ring dimer, a doubly H-bonded carboxyl-to-carboxyl structure, precludes formation of the six-membered ring OH + acid complex, above, and is therefore expected to be much less reactive toward OH, in accord with the observations.¹⁶

The major aim of the present study is to eliminate the existing contradictions in the temperature dependence of *k*₁ and to gain further insight into the precise mechanisms of the title reaction.

2. Experimental Section

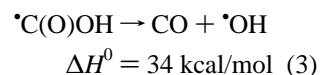
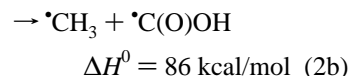
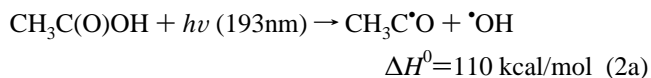
2.1. Pulsed Laser Photolysis–Pulsed Laser-Induced Fluorescence (PLP–PLIF) Technique. The PLP–PLIF experiments were carried out using a heatable, cylindrical, stainless-steel reactor of volume about 300 cm³ with burnished inner surfaces (see Figure 1). The reactor is equipped with five tubular stainless-steel arms, a gas inlet port, a gas outlet pipe leading via a throttle valve to a rotary pump, and three optical ports. Gas mixtures entered the reactor through the gas inlet port about 20 cm upstream of the photolysis region to ensure thermal equilibrium with the walls of the vessel and were pumped out through the gas outlet port located at the bottom of the central part of the reaction cell just in front of the fluorescence collection lens. The gas inlet consists of a ceramic tube of inner diameter 28 mm that is supported by a 60-cm-long fused silica quartz tube, which protrudes ca. 20 cm into the reactor along its axis. The ceramic tube has a SiC coating oxidized to chemically inert silica on the inner surface and two transverse opposite holes of 1.5 cm diameter near its end in order to allow the photolysis/probe laser beams to pass through the gas mixture within the ceramic tube at right angles to its axis. Its outside surface is surrounded by Ni/Cr resistive wire coils driven by an automatic digital temperature controller (EUROTHERMO), which enables the gas mixture in the probed volume to be heated

(Figure 1) to the desired temperature. The temperature of the gas mixture in the cell was measured using a J-type thermocouple that could be inserted, between kinetic measurements, into the reaction volume at the focus of the collecting lens where the laser beams pass. The pulsed emission from the 193 nm photolysis excimer laser (Lambda Physik COMPex 102) and the ca. 282 nm probe laser beam (Quantel DATACHROM-5000, YG 581-10, TDL 50) were coupled onto the same axis counter-propagating into the reaction volume through quartz windows located at the two designated optical ports of the reaction cell. These ports were equipped with series of 1-cm-diameter baffles to reduce stray light originating from the lasers. Through the third optical port, perpendicular to the aforementioned two ports, fluorescence was gathered by a 32-mm focal length quartz biconvex lens and imaged onto the active area of a photomultiplier (PMT, Hamamatsu R955) through a 310 ± 10 nm interference filter (Andover Corp.).

The pressure in the cell, monitored with 10, 100, and 1000 Torr capacitance manometers, was held constant at 50 or 100 Torr, using either Ar or N₂ as bath gases. Typical flow rates, regulated using calibrated mass flow controllers, were 300 sccm, resulting in linear gas velocities in the reaction cell between 12 and 33 cm s⁻¹, ensuring that a fresh gas sample was photolyzed at each laser pulse (rep. frequency 10 Hz).

The timing of the photolysis laser and the excitation laser was controlled using a PC digital time delay generator card (National Instruments) with a homemade electro-optic interface. The experiment was conducted in scan mode so that the delay between the lasers was incremented after each photolysis laser pulse at 10 Hz frequency. Typically, 50 data points were measured before the excimer laser fired, and 550 points afterward, resulting in a scan time of 60 s. The PMT signal, measured before the trigger signal for the excimer (i.e., in the absence of OH), was used to correct the OH fluorescence signal for scattered light from the excitation laser. Typically, 20 scans (1200 s) were then sufficient to obtain a good OH decay profile. The portion of the PMT signals containing the fast transient OH (A → X) fluorescence were gate-integrated by a boxcar (Stanford Research Systems SR250), then digitized by an A/D converter (ADC-12, PICO Technology Ltd.) and finally sent to a PC for further processing.

2.2. Generation and Detection of OH Radicals. OH was generated directly by the 193 nm (ArF excimer laser, 10 Hz repetition rate) photolysis of acetic acid. This photodissociation process may occur by multiple reaction channels, arising from cleavage of either the weaker C–C or the stronger C–O single bond, as given below with their energetics.²⁰ Two channels (2a, 3) may lead to OH:



It was concluded from photodissociation dynamics experiments by Naik et al.^{21,22} and Kwon et al.²³ that channel 2a predominates and that OH is formed with a quantum yield of 0.8, mainly in the ground vibrational state, because about 80% of the excess energy above the barrier is retained in the acetyl moiety.

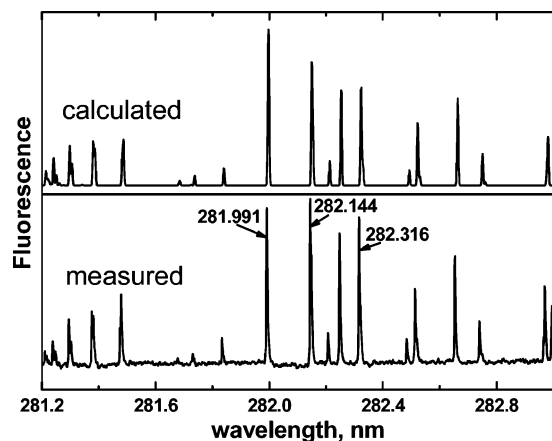


Figure 2. Measured and calculated LIF excitation spectrum of OH between 281.2 and 283 nm.

Typically, laser fluences of 200–900 $\mu\text{J}/\text{cm}^2$ per pulse were used to generate OH at concentrations between 10^{10} and 10^{11} molecules/ cm^3 , as calculated from

$$[\text{OH}] = (1/hc) \times \lambda \times f_L \times \sigma_{193} \times \Phi \times [\text{CH}_3\text{C}(\text{O})\text{OH}] \quad (4)$$

where h is Planck's constant, c is the light velocity, λ is the photolysis wavelength (193 nm), f_L is the excimer laser fluence, σ_{193} is the absorption cross section of $\text{CH}_3\text{C}(\text{O})\text{OH}$ at 193 nm ($1.1 \times 10^{-19} \text{ cm}^2$),²² and Φ is the quantum yield for OH formation (0.8).²² In some experiments, the initial concentration of OH was increased by a factor between 3 and 15 by varying the excimer pulse energy at the maximum $[\text{CH}_3\text{C}(\text{O})\text{OH}]$ concentration for the particular kinetic run at each temperature. The variation in excimer energy at the highest $[\text{CH}_3\text{C}(\text{O})\text{OH}]$ for the given run serves as a diagnostic for kinetic errors associated with secondary reactions of OH with either primary reaction products, or with products from the photolysis of the reactant (including another OH). No statistically significant difference was observed in the rate constants obtained over the range of this variation.

Fluorescence from OH $\text{A}^2\Sigma(v=1) \rightarrow \text{X}^2\Pi(v=1)$ at 310 ± 10 nm was detected following excitation of the $\text{A}^2\Sigma(v=1) \leftarrow \text{X}^2\Pi(v=0)$, $\text{Q}_{11}(1)$ transition at 281.997 nm. Laser radiation at that wavelength was provided by pumping rhodamine 590 dye in methanol by the second harmonic of the YAG laser (at 532 nm) and frequency doubling the ~ 564 nm dye laser output.

To select the most suitable wavelength for OH excitation, we measured the excitation spectrum (281.1–282.9 nm) of OH in 50 Torr Ar bath gas. The experiment was thus run in a synchronous scan mode in which the wavelength of the excitation laser was scanned at a fixed rate and OH fluorescence excited at a fixed delay after the excimer laser was collected at 10 Hz rate. The resulting spectrum at 296 K is given in Figure 2, along with a simulated excitation spectrum for the same temperature.²⁴ The OH $\text{A} \leftarrow \text{X}(1,0)$ excitation spectra at a given temperature were calculated assuming a Boltzmann distribution for population of the rotational levels in the $\text{X}^2\Pi(v'=0)$ electronic ground state. Figure 2 shows that the 281.997 nm transition is the most intense, is well separated from other rotational lines, and was therefore selected for our measurements.

2.3. Concentration of $\text{CH}_3\text{C}(\text{O})\text{OH}$. Special effort was made to measure the concentration of acetic acid accurately, the parameter most influential to the overall uncertainty in the measured rate coefficients. To deliver acetic acid into the reaction cell, a flow of Ar or N_2 carrier gas was passed through

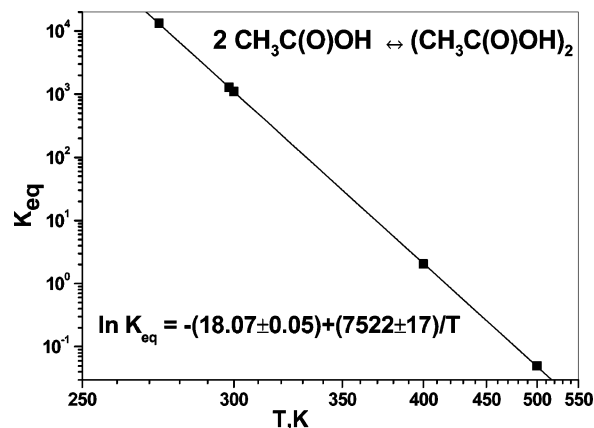


Figure 3. Temperature dependence of the equilibrium constant for dimerization of acetic acid based on Chao and Zwolinski data.²⁶ The line is our fit to the data, and uncertainties presented are one standard error.

a bubbler (see Figure 1) containing liquid acetic acid. The bubbler was placed in a large water bath at a temperature $T_b = 294 \pm 0.5$ K, about one degree below room temperature to ensure a stable temperature and to prevent condensation of acetic acid vapor before dilution with buffer gas. The total gas pressure (carrier plus acetic acid) over the liquid was maintained at $P_b = 700 \pm 20$ Torr. Before entering the reactor, the variable, calibrated flow of acetic acid in Ar or N_2 carrier was mixed with a calibrated flow of additional Ar or N_2 buffer.

The total number of moles of $\text{CH}_3\text{C}(\text{O})\text{OH}$ flowing out of the bubbler and passing through the reactor, Φ_{HAC} , can be derived from the known total vapor pressure of acetic acid, P_{aa} , duly taking into account the contributions of monomer and dimer

$$P_{\text{aa}} = P_{\text{bd}} + P_{\text{bm}} \quad (5)$$

which are governed by the equilibrium



with the equilibrium constant $K_{\text{eq}}(T_{(b)})$ at a given (bubbler) temperature, $T_{(b)}$, given by

$$\frac{K_{\text{eq}}(T_{(b)})}{P_0} = \frac{P_{\text{bd}}}{P_{\text{bm}}^2} \quad (7)$$

In these equations, P_{aa} , P_{bd} , and P_{bm} represent the vapor pressure of acetic acid and the partial pressures of the monomer and dimer (in the bubbler), respectively; P_0 is the standard pressure (750.06 Torr). The total vapor pressure P_{aa} is known accurately; it was calculated from the Antoine equation as presented in the NIST database²⁵

$$\log_{10} \frac{P_{\text{aa}}(\text{Torr})}{750.06} = 4.682 - \frac{1642.540}{T(\text{K}) - 39.764} \quad (8)$$

valid in the $T = 290$ – 391 K range. The equilibrium constant $K_{\text{eq}}(T)$ was calculated from

$$\ln K_{\text{eq}}(T) = -(18.07 \pm 0.05) + \frac{(7522 \pm 17)}{T(\text{K})} \quad (9)$$

which is our fit to the data of Chao and Zwolinski²⁶ for the temperature range 273–500 K, presented in Figure 3. Equations 5 and 7 lead to the following expression for P_{bm}

$$P_{\text{bm}} = \frac{P_0}{2 \times K_{\text{eq}}(T_{\text{b}})} \times \left(\left[1 + 4 \times K_{\text{eq}}(T_{\text{b}}) \times \frac{P_{\text{aa}}}{P_0} \right]^{1/2} - 1 \right) \quad (10)$$

from which P_{bd} can be calculated using eqs 5 and 8. Note that at $T_{\text{b}} = 294\text{ K}$, $P_{\text{bd}} = 11.0\text{ Torr}$ and $P_{\text{bm}} = 2.2\text{ Torr}$, that is, the dimer is preponderant in the bubbler.

The number of moles of acetic acid flowing out of the bubbler and hence also through the reactor per unit time, Φ_{HAc} , can then be found from

$$\Phi_{\text{HAc}} = F_{\text{b}} \times \frac{P_{\text{s}}}{RT_{\text{s}}} \times \frac{P_{\text{bm}} + 2 \times P_{\text{bd}}}{P_{\text{b}}} = F_{\Sigma} \times \frac{P_{\text{s}}}{RT_{\text{s}}} \times \frac{P_{\text{m}} + 2 \times P_{\text{rd}}}{P_{\Sigma}} \quad (11)$$

Here, F_{b} and F_{Σ} represent the total gas flows through the bubbler and the reactor, respectively, expressed at reference pressure P_{s} and temperature T_{s} ; P_{b} and P_{Σ} are the total pressure in the bubbler and the reactor; P_{m} and P_{rd} are the monomer and dimer partial pressures in the reactor; R is the gas constant. Using eq 11, one finds the *weighted* sum of acetic acid pressures in the reactor, $P_{\text{wr}} \equiv P_{\text{m}} + 2P_{\text{rd}}$, as follows:

$$P_{\text{wr}} = (P_{\text{bm}} + 2 \times P_{\text{bd}}) \times \frac{P_{\Sigma}}{P_{\text{b}}} \times \frac{F_{\text{b}}}{F_{\Sigma}} \quad (12)$$

From P_{wr} and using the equilibrium expression (eq 7) adapted to the conditions of the reactor, one obtains the expression for P_{rm} , at the reactor temperature T_{r}

$$P_{\text{rm}} = \frac{P_0}{4 \times K_{\text{eq}}(T_{\text{r}})} \times \left(\left[1 + 8 \times K_{\text{eq}}(T_{\text{r}}) \times \frac{P_{\text{wr}}}{P_0} \right]^{1/2} - 1 \right) \quad (13)$$

whereas P_{rd} is obtained from $P_{\text{wr}} \equiv P_{\text{m}} + 2 \times P_{\text{rd}}$. Finally, the concentration of acetic acid monomer in the reactor, $[\text{CH}_3\text{C}(\text{O})\text{OH}]$, was derived from P_{rm} through the gas law: $[\text{CH}_3\text{C}(\text{O})\text{OH}](\text{molecule cm}^{-3}) = P_{\text{rm}}(\text{Torr}) \times 3.26 \times 10^{16} \times 296/T_{\text{r}}$, and the number fraction of the monomer in the reactor, $f_{\text{m}} \equiv P_{\text{m}}/(P_{\text{m}} + P_{\text{rd}})$, was calculated from P_{m} and P_{rd} as derived above. Note that the reactor monomer fraction always approached unity: $0.82 < f_{\text{m}} < 1$, because of the dilution effect, $F_{\Sigma} \gg F_{\text{b}}$, and the (mostly) higher reactor temperature T_{r} compared to the bubbler temperature $T_{\text{b}} = 294\text{ K}$. For reaction temperatures $T_{\text{r}} > 350\text{ K}$, f_{m} was always > 0.995 (see Table 1).

It should be emphasized that the above approach to determine the concentration of acetic acid in the reactor is valid only if the outgoing flow of acetic acid from the bubbler does not disturb the equilibrium gas-phase concentration of acetic acid over the liquid phase in the bubbler. At vapor/liquid equilibrium, the vaporization and condensation processes that control the gas-phase concentration of the species under consideration are in exact balance, with the rate of condensation, in mol/unit time, given by

$$J = [n \times \langle c \rangle / 4] \times \alpha \times S / N_{\text{A}} \quad (14)$$

where n is the gas-phase number density of species, $\langle c \rangle$ is its average molecular velocity, α is the mass accommodation coefficient or the probability of uptake of a gaseous molecule when colliding with the liquid surface, S is the liquid-phase area exposed to the gas phase in the bubbler (at least the static area of 12.6 cm^2), and N_{A} is Avogadro's number. According to IUPAC,¹⁹ α usually ranges from 1 to $\sim 10^{-2}$. Even when adopting an extremely low α value of 10^{-3} , J is calculated to

be $\sim 10^{-4}$ mol/sec, that is, 2 orders of magnitude greater than the largest outgoing flow of acetic acid from the bubbler, $\Phi_{\text{HAc}} \approx 1.2 \times 10^{-6}$ mol/sec at the highest experimental F_{b} of 50 sccm. This means that the vapor/liquid equilibrium in the bubbler is always maintained at better than 99%. Another implicit assumption above is that the dimer/monomer equilibrium adapts to the reaction-zone conditions of higher temperature and higher dilution in a time much shorter than the time $\tau_{\text{res}} \approx 1\text{ s}$ the gas mixture spends in the 15-cm-long heated ceramic tube (linear flow velocity of $\sim 20\text{ cm/s}$; see above). The $\{[\text{dimer}]/[\text{monomer}]\}_{\text{eq}}$ relaxation time, τ_{rel} , is approximated by the reciprocal of the dimer dissociation rate constant k_{-6} . According to transition state theory: $k_{-6} \geq (k_{\text{b}}T_{\text{r}}/h) \times \exp(-E_{\text{d}}/RT_{\text{r}})$, where k_{b} and h are the Boltzmann and Planck constants, respectively, and E_{d} is the dimerization energy ($\sim 15\text{ kcal/mol}$; see eq 9). It thus follows that, for example, for $T_{\text{r}} = 400\text{ K}$, $\tau_{\text{rel}} \leq 2 \times 10^{-5}\text{ s}$, which is indeed many orders of magnitude less than τ_{res} . A final requirement for accurate concentration determinations based on acetic acid flows is that there be no loss of this species while it flows from the bubbler to the reaction region. In our closed, flow-through system, with all contact surfaces Teflon, Pyrex, or silica, the only conceivable loss process is adsorption to the walls, which lasts only until the adsorption-desorption equilibrium is reached. Establishment of a new equilibrium after each acetic acid flow change was verified prior to the rate-constant measurement, as detailed in subsection 3.2.

2.4. Chemicals. N₂, Ar (both Messer 5.0, 99.999%), and CH₃C(O)OH (Aldrich, purity greater than 99.99%) were used without further purification.

3. Results and Discussion

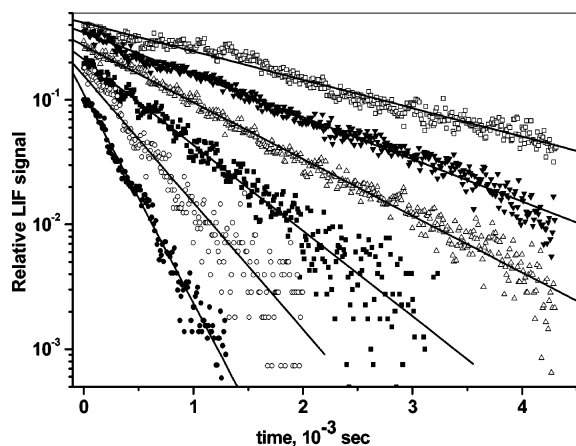
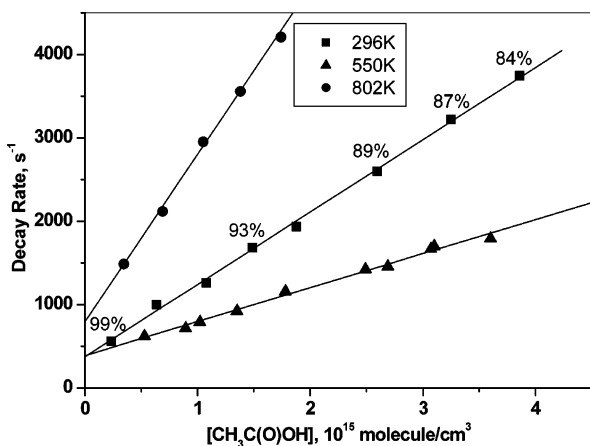
3.1. Kinetics of OH + CH₃C(O)OH. The PLP-PLIF OH decay studies were carried out under pseudo-first-order conditions, that is, $[\text{CH}_3\text{C}(\text{O})\text{OH}] \gg [\text{OH}]$. Fluorescence decays of OH were fitted to a single-exponential function to obtain the pseudo-first-order OH-decay rate. At each temperature, the rate constant, $k_1(T)$, was determined from the slope of a plot of the OH-decay rate versus the monomer acetic acid concentration $[\text{CH}_3\text{C}(\text{O})\text{OH}]$, varied over a wide (usually 10-fold) range. The rate constants, $k_1(T)$, obtained at each temperature, along with information on the reactant concentration and monomer fraction range, pseudo-first-order decay rates, and the number of decay runs, are presented in Table 1. Figure 4 shows OH decays measured at different excess concentrations of CH₃C(O)OH at 296 K. Figure 5 displays examples of plots of the pseudo-first-order decay rates versus $[\text{CH}_3\text{C}(\text{O})\text{OH}]$ at different temperatures. Within experimental uncertainty, the measured rate coefficients were found to be independent of the variation of bath gas pressure between 50 and 100 Torr of Ar or N₂. Thus, in the present work, absolute kinetic data on the reaction of OH with CH₃C(O)OH have been obtained for the wide temperature range 287–802 K, including, as far as we are aware, the first data at temperatures above 450 K. The rate constant data are plotted in Arrhenius form in Figure 6, along with the other available data from the literature for the title reaction.

3.2. Comparison with Literature Values of k_1 and Assessment of Monomer and Dimer Concentration Determinations Affecting the k_1 Data. Table 2 summarizes the experimental $k_1(T)$ data available in the literature. As can be seen in Figure 6, three temperature-dependent studies, including ours, clearly indicate a negative temperature dependence of k_1 for T up to 450 K. The only study reporting a positive temperature dependence of k_1 is that of Dagaut et al.¹⁷ This discrepancy has been discussed first by Singleton et al.,¹⁶ who suggested that

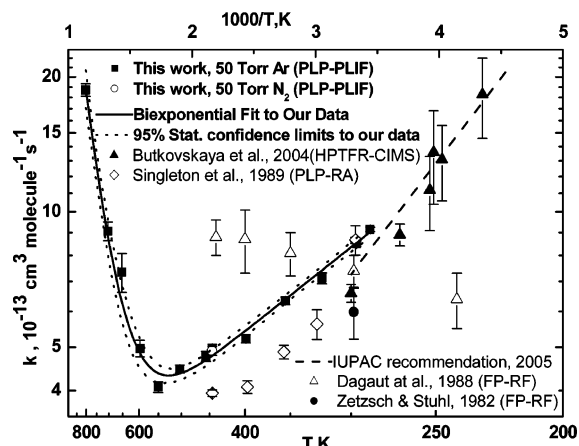
TABLE 1: Rate Constants Measured in the Present Work for the Reaction of OH with CH₃C(O)OH

<i>T</i> , K	[CH ₃ C(O)OH], 10 ¹⁴ molecules cm ⁻³	no. ^a	monomer number fraction <i>f</i> _m , %	decay rates, s ⁻¹	<i>k</i> (<i>T</i>) ₁ , ^b 10 ⁻¹³ cm ³ molecule ⁻¹ s ⁻¹
287	3.44–19.7 (3.44–19.4) ^c	9	96–82 (96–81)	647–2237	9.15 ± 0.11 ^d
296	1.30–38.60 (1.30–37.74) ^c	46	99–84 (99–83)	375–3744	8.49 ± 0.12 ^e
322	2.01–46.50	17	≥97	380–3335	7.12 ± 0.20
355	2.94–54.90	22	≥99.5	455–3732	6.34 ± 0.12
399	1.27–15.46	16	≥99.9	391–1149	5.22 ± 0.11
446	1.14–38.68	25	≥99.99	369–1982	4.98 ± 0.09 ^f
456	2.23–61.89	17	≥99.99	502–3289	4.77 ± 0.12
503	4.64–68.14	24	≥99.99	542–3320	4.47 ± 0.09
550	5.28–31.53	10	≥99.99	622–1667	4.08 ± 0.11
597	4.08–47.55	22	≥99.99	745–3313	4.97 ± 0.21
653	1.77–8.83	4	≥99.99	582–1113	7.35 ± 0.73
703	1.65–31.53	9	≥99.99	728–3732	9.06 ± 0.44
802	3.45–17.39	27	≥99.99	722–4207	18.7 ± 0.60

^a Number of (different) experimental CH₃C(O)OH concentrations. ^b Stated errors represent the statistical standard deviation and do not include an estimated uncertainty of ~8% associated with possible systematic errors. ^c Values in parentheses calculated from eq 15 as used by Butkovskaya et al.¹⁴ ^d Averaged value includes results 9.13 ± 0.57 in N₂, 100 Torr. ^e Averaged value includes results 8.65 ± 0.14 in N₂, 50 Torr. ^f Averaged value includes results 4.91 ± 0.11 in N₂, 50 Torr.

**Figure 4.** Examples of OH decays for the OH with acetic acid reaction at 296 K.**Figure 5.** Pseudo-first-order OH decay rate versus concentration of CH₃C(O)OH from experiments at 296, 550, and 802 K. Monomer number fractions *f*_m at 296 K are indicated in percent. At 550 and 802 K, *f*_m ≥ 99.9%. Error bars are masked by the symbol size.

strong adsorption of the carboxylic acid on the glass bulb walls of the milli-Torr-range stock mixtures used by Dagaut et al. might have affected the CH₃C(O)OH concentration determinations in that work. Note that in our experiments between 5 and 10 min were necessary to establish a new equilibrium concentration of acetic acid in the reactor after changing its flow rate; this was

**Figure 6.** Arrhenius plot of the determined rate constants for the reaction of OH with CH₃C(O)OH from this study and studies by other groups. The statistical 95% confidence limits in the fit to our data (solid line) are represented by the dotted lines. Error bars are two standard errors as quoted by the authors. Our data points at 287 K (N₂, 100 Torr) and 296 K (N₂, 50 Torr) are omitted for sake of clarity.

verified by using the intensity of the OH(A → X) fluorescence, at a fixed, short delay between the photolysis and probe beams, as a direct measure for the relative concentration of CH₃C(O)OH in the reaction zone. The value of *k*₁ reported by Zetsch and Stuhl²⁷ is the lowest among all room-temperature measurements reported so far. The recent room-temperature value from Butkovskaya et al.¹⁴ is also less than ours by 22%. Those authors attributed their estimated error of ~17% mainly to the uncertainty of the monomer/dimer equilibrium constant, for which they adopted the expression

$$\ln K_{\text{eq}}(T) = -(17.36 \pm 0.13) + \frac{(7290 \pm 144)}{T(\text{K})} \quad (15)$$

which differs somewhat from eq 8 used in our work. We have therefore recalculated the acetic acid concentrations and monomer fractions in our study using eq 15. As can be seen from Table 1, the discrepancies between the concentrations derived for 296 K using eqs 8 and 15 do not exceed 2.2% even at our highest monomer [CH₃C(O)OH] of 3.86 × 10¹⁵ molecules/cm³ or lowest 84% monomer number fraction. The presence of dimer in our experiments (16% at worse case) should have little

TABLE 2: Summary of Room-Temperature Rate Constants and Arrhenius Parameters from Studies of the OH Reaction with Acetic Acid

temp range, K	$k_1(\text{room temp})^a$ $10^{-13}\text{ cm}^3\text{molecule}^{-1}\text{s}^{-1}$	A_1 $10^{-14}\text{ cm}^3\text{molecule}^{-1}\text{s}^{-1}$	$E/R \pm \Delta E/R$, K	ref (technique) ^b
298	5.99 ± 0.78			27 (FP–RF)
240–440	7.40 ± 0.60 (298 K)	130	170 ± 20	17 (FP–RF)
297–446	8.67 ± 0.65 (297 K)			16 (PLP–RA)
229–300	6.60 ± 1.10 (300 K)	2.2	-1012 ± 80	14 (HPTFR–CIMS)
287–802	8.50 ± 0.9 (296 K)	2.9×10^{5c} 15.0	6030 ± 780 -515 ± 30	this work

^a Uncertainties as quoted by the authors. The uncertainty for the present work includes an estimated systematic error of 8% beside the statistical standard deviation. ^b Abbreviations for the techniques used in the references cited are widely adopted by IUPAC.¹⁹ ^c Experimental rate constant given by sum $k_1(T) = A_1 \times \exp(-E_1/RT) + A_2 \times \exp(-E_2/RT)$.

influence in terms of its competition for OH. Indeed, using the rate constant $k_d(295\text{ K}) \approx 10^{-14}\text{ cm}^3\text{ molecule}^{-1}\text{ s}^{-1}$ for the reaction of OH with acetic acid dimer as measured by Singleton et al.,¹⁶ our worst-case ratio $k_d[\text{dimer}]/k_1[\text{monomer}]$ is found to be $(0.16/0.84) \times (10^{-14}/8.5 \times 10^{-13}) = 0.002$. Moreover, most of our kinetic experiments at room temperature were conducted for acetic acid monomer fractions above 92%, and even greater than 99.5% for higher temperature runs. The linearity of the decay rate versus monomer $[\text{CH}_3\text{C}(\text{O})\text{OH}]$ plot at 296 K up to the highest data point for 84% monomer shown in Figure 5 serves as a clear demonstration that the higher $[\text{CH}_3\text{C}(\text{O})\text{OH}]$, employed to improve the accuracy of the rate constants, can be reached without affecting the validity of the experimental procedure, thereby confirming the low k_d/k_1 ratio found by Singleton et al.¹⁶ The unexplained discrepancy between our k_1 –(296 K) value and that of Butkovskaya et al.¹⁴ should not cause grave concern because the difference is within the combined uncertainties of 20–30%; more important is that the $k_1(T)$ data of our two studies show a closely similar trend. The room-temperature rate constant reported by Singleton et al.¹⁶ is in excellent agreement with ours. In fact, their experimental approach was quite similar to ours, using photolysis of acetic acid as a source of OH and adopting a similar expression for the dimerization equilibrium constant $K_{\text{eq}}(T)$, but their acetic acid concentrations were one to two orders of magnitude higher than those used in this study. Their observed trend of k_1 with temperature in the range of 325–450 K is also similar to ours, although the absolute $k_1(T)$ data differ from 3 to 20%, which might be linked to the great difference in the acetic concentrations used.

3.3. Mechanistic Interpretation of the Temperature Dependence of $k_1(T)$. Our $k_1(T)$ results over the entire temperature range 287–802 K can be represented well by the biexponential expression

$$k_1(T) = 2.9 \times 10^{-9} \exp(-6030/T) + 1.50 \times 10^{-13} \exp(515/T) \text{ cm}^3 \text{ molecule}^{-1} \text{ s}^{-1} \quad (16)$$

with 95% statistical confidence limits averaging $\pm 4\%$ below 550 K and $\pm 10\%$ above 550 K (see Figure 6), and systematic errors estimated at $\pm 8\%$ throughout. The $k_1(T)$ data, exhibiting a pronounced minimum, near 530 K, and showing strongly diverging trends in the low- and high-temperature regions, can only be rationalized by a change in the reaction mechanism as a function of temperature.

The distinct negative temperature dependence observed below 500 K is in line with the determinations by Singleton et al.¹⁶ and by Butkovskaya et al.¹⁴ As shown in the recent work by

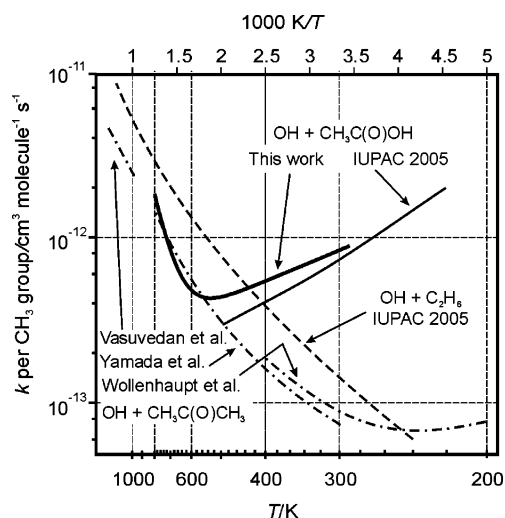
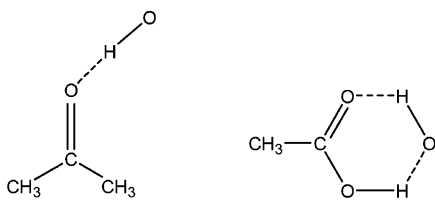


Figure 7. Temperature dependences of rate constants *per CH₃ group* for OH reactions with ethane, acetone, and acetic acid monomer. Data for acetone from refs 28, 29, and 30, and those for ethane from ref 31. With OH + C₂H₆ as the reference reaction, the effects of H-bonding on the rate constants for OH + CH₃C(O)CH₃ and, more so, for OH + CH₃C(O)OH are clear. For T above 800 K, $k(\text{OH} + \text{CH}_3\text{C}(\text{O})\text{OH})$ is expected to increase less steeply and follow a trend close to $k(\text{OH} + \text{C}_2\text{H}_6)$ and $k(\text{OH} + \text{CH}_3\text{C}(\text{O})\text{CH}_3)$.

Vereecken et al.,¹⁵ this “low-temperature” behavior is in agreement with an H-abstraction mechanism proceeding through H-bonded pre-reactive complexes and strongly enhanced by tunneling. The most stable complex (ca. -7.3 kcal/mol relative to the reactants¹⁵) is a six-membered ring featuring two H bonds between OH and the carboxyl group (see Figure 8) favoring abstraction of the acidic H. This rather unusual mechanism, the carboxyl O–H bond being $\sim 12\text{ kcal/mol}$ stronger than the methyl C–H bonds,¹⁵ was experimentally confirmed by the measured acidic/methyl H-abstraction ratio of 2:1 at room temperature.^{14,15} The pronounced increase of $k_1(T)$ at lower temperatures is due mainly to the slower complex redissociation back into the reactants, such that a larger fraction of the complexes formed will be stabilized and can undergo H-abstraction by tunneling through the barrier to the low-lying CH₃C(O)O–HOH postreaction complex.¹⁵

The impact of the pre-reactive double H-bonding on the rate coefficient $k_1(T)$ of the title reaction is demonstrated by a comparison with the $k(T)$ -behavior for the OH reactions with acetone^{28–30} and with ethane,³¹ shown in Figure 7, which displays the rate coefficients *per methyl group*, that is, $1/2 k(T)$ for both OH + acetone and OH + ethane. Similar to OH + acetic acid, the low-temperature reaction of OH + acetone may



Acetone H-bonded complex Acetic Acid H-bonded complex

Figure 8. Pre-reactive H-bonded complexes formed in the course of reaction of OH with acetone and acetic acid.

likewise proceed through a pre-reactive complex,⁸ but one that features only a single H bond (see Figure 8) and, accordingly, has a stability (ca. 4 kcal/mol⁸) only about half that of the complex for the title reaction.¹⁵ However, no pre-reactive complex is expected for OH + ethane, which can proceed only by direct H-abstraction. The drastic differences in the low-temperature values and T dependences of the three rate coefficients at issue, shown in Figure 7, are in line with the existence of pre-reactive complexes and their stabilities. Although $k(\text{OH} + \text{ethane})$ exhibits a “normal” positive T -dependence and becomes very small at lower temperatures, $k(\text{OH} + \text{acetone})$ levels off at $\sim 1.4 \times 10^{-13} \text{ cm}^3 \text{ molecule}^{-1} \text{ s}^{-1}$ around $T_{\text{min}} \approx 250 \text{ K}$, and even appears to increase again as T drops further.²⁸ For OH + CH₃C(O)OH, the low-temperature $k_1(T)$ is over an order of magnitude higher than even that for acetone, shows a much more pronounced negative T -dependence, and exhibits its minimum at $T_{\text{min}} \approx 530 \text{ K}$, that is, almost double the T_{min} of $\sim 250 \text{ K}$ for acetone, reflecting the ca. twice larger stability of the OH- -acetic acid complex, such that it can survive up to higher T .

At very high temperatures $>1000 \text{ K}$, however, the title reaction is expected to proceed through direct methyl-H-abstraction, as for the reaction of OH with ethane. Note that the small differences in the $D_0(\text{C}-\text{H})$ bond energies, with the CH₃C(O)OH value ($\sim 96 \text{ kcal/mol}$) intermediate to those in CH₃C(O)CH₃ ($\sim 93.5 \text{ kcal/mol}$) and in CH₃CH₃ ($\sim 99.5 \text{ kcal/mol}$),³² are due to vinyloxy-type resonances in the product radicals from the former two, resonances that are not yet active in the “early” transition states for the exoergic H-abstractions at issue,³² such that the barriers for the direct H-abstractions are not expected to differ significantly. Therefore, it is reasonable to expect that $k_1(T)$ for $T > 1000 \text{ K}$ has a value close to the $k(T)$ for OH + CH₃CH₃ and OH + CH₃C(O)CH₃ *per CH₃ group*. As shown in Figure 7, our $k_1(T)$ results near 800 K do indeed approach the expected values, but are substantially lower at temperatures of 550–750 K. This apparent dip in reactivity at these intermediate temperatures might be explained in terms of the dynamics of the process, which should still be influenced by the relatively deep potential energy well ($\sim 7.3 \text{ kcal/mol}$) of the doubly-H-bonded complex between OH and the carboxyl moiety. Thus, an OH-radical approaching the CH₃ moiety will be deviated toward the C(O)OH group and may even be captured by it, but, at these temperatures, not long enough to rearrange the bonds in the complex for H-abstraction; instead, the complex should redissociate rapidly, expelling the OH in a general direction away from the CH₃ group. Such a possible rate-inhibiting effect by (potential) H-bonding was suggested already by Smith and Ravishankara.³³ However, at still higher temperatures ($>1000 \text{ K}$), the OH moves too fast to be substantially deviated to the C(O)OH group, and can therefore efficiently attack the CH₃ moiety in a direct methyl-H-abstraction. Thus, because there appears to be no viable rationalization for the direct abstraction of a methyl-H from CH₃C(O)OH to be significantly faster than from ethane or

acetone, one must expect $k_1(T)$ to increase less steeply at temperatures $>800 \text{ K}$ so as to get in line with the high- T rate constant behavior for the direct methyl-H abstractions from ethane and acetone. Clearly, $k_1(T)$ measurements at temperatures above 800 K are awaited to verify these views. Note that according to the views above on the two faces of hydrogen bonding, channels 1a and 1b are not independent; therefore, one cannot extract Arrhenius-type expressions for the two channel rate coefficients k_{1a} and k_{1b} solely from the overall $k_1(T)$ data, even when available over a wide T -range, as at present. Only experimental determinations of the k_{1a}/k_{1b} branching ratio as a function of temperature, combined with $k_1(T)$, can provide this information. To that end, molecular beam sampling–mass spectrometry product measurements¹⁵ over a wide T -range are being set up in this laboratory.

The question may arise whether in the present experimental conditions the pre-reactive complex is collisionally thermalized or chemically activated. According to results of our earlier theoretical study,¹⁵ the lifetime of the complex at 300 K can be roughly estimated at several tens of nanoseconds, that is, long enough for near-thermalization at pressures of 50–100 Torr. In any case, as can be shown theoretically, the rate constant for this type of complex-assisted reaction with the TS for the final H-abstraction lying above the reactants level should not show significant pressure dependence,³⁴ in agreement with the current and earlier^{14,16} findings.

3.4. Atmospheric Implications. Given the high observed acetic acid mixing ratios, f , up to a few hundred parts per trillion in the upper troposphere (UT),³⁵ and with k_1 around $1.5 \times 10^{-12} \text{ cm}^3 \text{ molecule}^{-1} \text{ s}^{-1}$ at the prevailing temperatures of 220–250 K, the importance of the OH + CH₃C(O)OH reaction in the UT approaches that of OH + CH₄ ($f_{\text{CH}_4} = 1.8 \text{ ppm}$, and $k_{\text{CH}_4+\text{OH}}$ around 1×10^{-15} at 220–250 K¹⁸). Therefore, the impact of the title reaction on the HOx radical budget in the UT deserves closer attention. The mechanistic considerations above indicate that the OH + CH₃C(O)OH reaction at free-troposphere temperatures, 270 K down to 220 K, should yield dominantly CH₃C(O)O• + H₂O. Therefore, we must address the likely fate of the acetyloxy radical and the subsequent reaction pathways. As mentioned in the Introduction, the sole fate of CH₃C(O)O• under all tropospheric conditions is expected to be its dissociation into CH₃ + CO₂ because the barrier for this reaction was found to be only $\sim 5 \text{ kcal/mol}$.¹³ Thus, interestingly, the subsequent chemistry of the OH-initiated oxidation of acetic acid in the free and upper troposphere should be identical to that of the methane oxidation. The relative importance of these two reactions in the UT, using the rate coefficient data at 220–250 K above, and adopting a acetic acid mixing ratio of 200 ppt, can be evaluated as $k_1 [\text{CH}_3\text{C(O)OH}]/k_{\text{CH}_4} [\text{CH}_4] = 0.17$. Therefore, under these conditions, acetic acid contributes significantly to the formation of CH₃O₂ radicals and hence also affects the HOx budget, depending on whether CH₃O₂ reacts mainly with NO to produce formaldehyde, a photolytic HOx source, or, at low [NO], reacts with HO₂ in a termination step to yield CH₃OOH.

Acknowledgment. This work was sponsored by the Belgian Science Policy Office through the Research Programs Global Change and Sustainable Development and Science for Sustained Development, and by the European Commission through the FP5 Program, Environment & Climate project Utopihan-Act. S.A.C. and J.P. are also indebted to the Fund for Scientific Research Flanders (FWO) and to the KULeuven Research

Council (BOF and GOA programs) for continuing financial support through postdoctoral mandates and research projects.

References and Notes

- Andrae, M. O.; Talbot, R. W.; Andrae, T. W.; Harris, R. C. *J. Geophys. Res.* **1998**, *93*, 1616.
- Talbot, R. W.; Mosher, B. W.; Heikes, B. G.; Jacob, D. J.; Munger, B. C.; Daube, B. C.; Keene, W. C.; Maben, J. R.; Artz, R. S. *J. Geophys. Res.* **1995**, *100*, 9335.
- Kawamura, K.; Ng, L.; Kaplan, I. R. *Environ. Sci. Technol.* **1985**, *19*, 1082.
- Talbot, R. W.; Andrae, M. O.; Berressein, H.; Jacob, D. J.; Beecher, K. M. *J. Geophys. Res.* **1990**, *95*, 16799.
- Enders, G.; Dlugi, R.; Steinbrecher, R.; Clement, B.; Daiber, R.; Eijik, J. V.; Gab, S.; Haziza, M.; Helas, G.; Hermann, U.; Kessel, M.; Kesselmeier, J.; Kotzias, D.; Kourtidis, K.; Kurth, H. H.; McMillen, R. T.; Roider, G.; Schurmann, W.; Teichmann, U.; Torres, L. *Atmos. Environ.* **1992**, *26*, 171.
- Dibb, J. E.; Arsenaault, M. *Atmos. Environ.* **2002**, *36*, 2513.
- Warneck P. *J. Atmos. Chem.* **2005**, *51*, 119.
- Vandenberk, S.; Vereecken, L.; Peeters, J. *Phys. Chem. Chem. Phys.* **2002**, *4*, 461.
- Talukdar, R. K.; Gierczak, T.; McCabe, D. C.; Ravishankara, A. R. *J. Phys. Chem. A* **2003**, *107*, 5021.
- Wollenhaupt, M.; Crowley, J. N. *J. Phys. Chem. A* **2000**, *104*, 6429.
- (a) Hermans, I.; Nguyen, T. L.; Jacobs, P. J.; Peeters, J. *J. Am. Chem. Soc.* **2004**, *126*, 9908. (b) Hermans, I.; Müller, J. F.; Nguyen, T. L.; Jacobs, P. A.; Peeters, J. *J. Phys. Chem. A* **2005**, *109*, 4303.
- Grosjean, D. *Environ. Sci. Technol.* **1989**, *23*, 1506.
- Peeters, J.; Fantechi, G.; Vereecken, L. *J. Atmos. Chem.* **2004**, *48*, 59.
- Butkovskaya, N. I.; Kukui, A.; Pouvesle, N.; Le Bras, G. *J. Phys. Chem. A* **2004**, *108*, 7021.
- De Smedt, F.; Bui, X. V.; Nguyen, T. L.; Peeters J.; Vereecken, L. *J. Phys. Chem. A* **2005**, *109*, 2401.
- Singleton, L.; Paraskevopoulos, G.; Irwin, R. S. *J. Am. Chem. Soc.* **1989**, *111*, 5248.
- Dagaut, P.; Wallington, T. J.; Liu, R.; Kurylo, M. J. *Int. J. Chem. Kinet.* **1988**, *20*, 331.
- Sander, S. P.; Friedl, R. P.; Ravishankara, A. R.; Golden, D. M.; Kolb, C. E.; Kurylo, M. J.; Huie, R. E.; Orkin, V. L.; Molina, M. J.; Moortgat, G. K.; Finlayson-Pitts, B. J. *Chemical Kinetics and Photochemical Data for Use in Stratospheric Modeling*; Jet Propulsion Laboratory publication 02-25, Evaluation 14, California Institute of Technology, 2003; <http://jpldataeval.jpl.nasa.gov/>.
- (19) *Summary of Evaluated Kinetic and Photochemical Data for Atmospheric Chemistry* and accompanying Heterogeneous Data Sheets, IUPAC subcommittee for gas kinetic data evaluation: <http://www.iupac-kinetic.ch.cam.ac.uk/>, 2005.
- (20) *CRC Handbook of Chemistry and Physics*, 80th ed.; Linde, D. R., Ed.; CRC Press: Boca Raton, FL, 1999.
- (21) Naik, P. D.; Upadhyaya, H. P.; Kumar, A.; Sapre, A. V.; Mittal, J. *P. Chem. Phys. Lett.* **2001**, *340*, 116.
- (22) Naik, P. D.; Upadhyaya, H. P.; Kumar, A.; Sapre, A. V.; Mittal, J. *P. J. Photochem. Photobiol., C* **2003**, *3*, 165.
- (23) Kwon, H. T.; Shin, S. K.; Kim, S. K.; Kim, H. L.; Park, C. R. *J. Phys. Chem. A* **2001**, *105*, 6775.
- (24) Luque, J.; Crosley, D. R. *LIFBASE: Database and Spectral Simulation Program*, version 1.5; SRI International Report MP 99-009, 1999.
- (25) NIST Standard Reference Database Number 69, June 2005 release, <http://webbook.nist.gov/chemistry/>.
- (26) Chao, J.; Zwolinski, B. J. *J. Phys. Chem. Ref. Data* **1978**, *7*, 363.
- (27) Zetzsch, C.; Stuhl, F. *Phys. Chem. Behav. Atmos. Pollut., Proc. Eur. Symp.* **1982**, 69.
- (28) Wollenhaupt, M.; Carl, S. A.; Horowitz, A.; Crowley J. N. *J. Phys. Chem. A* **2000**, *104*, 2695.
- (29) Yamada, T.; Taylor, Ph.; Goumri, A.; Marshall, P. *J. Chem. Phys.* **2003**, *119*, 10600.
- (30) Vasudevan, V.; Davidson, D. F.; Hanson, R. K. *J. Phys. Chem. A* **2005**, *109*, 3352.
- (31) Baulch, D. L.; Bowman C. T.; Cobos, C. J.; Cox, R. A.; Just, T.; Kerr, J. A.; Pilling, M. J.; Stocker, D.; Troe, J.; Tsang, W.; Walker, R. W.; Warnatz, J. *J. Phys. Chem. Ref. Data* **2005**, *34*, 757.
- (32) Vereecken, L.; Peeters, J. *Phys. Chem. Chem.* **2002**, *4*, 467.
- (33) Smith, I. W. M.; Ravishankara, A. R. *J. Phys. Chem. A* **2002**, *106*, 4798.
- (34) Peeters, J.; Vereecken, L. *Hydrogen abstractions by OH radicals through H-bonded complexes: pressure dependence?* 19th International Symposium on Gas Kinetics Proceedings; Orléans, France, July 2006; Dagaut, Ph., Mellouki, A., Eds.; p 147; manuscript in preparation.
- (35) Chapman, E. G.; Kenny, D. V.; Busness, K. M.; Thorp, J. M.; Spicer, C. W. *Geophys. Res. Lett.* **1995**, *22*, 405.